Direct *Operando* Identification of Reactive Electron Species Driving Photocatalytic Hydrogen Evolution on Metal-loaded Oxides

Hiromasa Sato†, Toshiki Sugimoto*, †, ‡

†Department of Materials Molecular Science, Institute for Molecular Science, Okazaki, Aichi 444-8585, Japan

‡Graduate Institute for Advanced Studies, SOKENDAI, Okazaki, Aichi 444-8585, Japan

*e-mail: toshiki-sugimoto@ims.ac.jp

KEYWORDS. Operando infrared spectroscopy, Reactive species, Photocatalysis, Hydrogen evolution, Metal cocatalyst

ABSTRACT: Performing *operando* spectroscopy under practical reaction conditions and extracting spectral components correlating with reaction activity are crucial in elucidating the reactive species in photocatalysis. However, the observation of weak signals corresponding to reactive photogenerated species is frequently hampered under reaction conditions owing to intense background signals originating from thermally-induced species unrelated to the photoinduced reactions. Herein, by synchronizing the millisecond periodic excitations of photocatalysts with a Michelson interferometer used for FT–IR spectroscopy, we succeeded in significantly suppressing the signals derived from thermally excited electrons and observing the reactive photogenerated electrons contributing to the photocatalytic hydrogen evolution. This demonstration was achieved for metal-loaded Ga_2O_3 photocatalysts under steam methane reforming conditions. Although it has long been conventionally believed that loaded metal cocatalysts function as sinks for reactive photogenerated electrons and active sites for reduction reactions, we found that the free electrons in the metal cocatalysts were not directly involved in the reduction reaction. Alternatively, the electrons shallowly trapped in the in-gap states of Ga_2O_3 contributed to enhancing the hydrogen evolution rate upon the loading of metal cocatalysts. We verified that the electron abundance in the in-gap states was clearly correlated to the reaction activity, suggesting that metal-induced semiconductor surface states formed in the periphery of the metal cocatalyst play key roles in the photocatalytic hydrogen evolution. Our microscopic insights shift a paradigm on the traditionally believed role of metal cocatalysts in photocatalysis and provide a fundamental basis for rational design of the metal/oxide interfaces as promising platforms for non-thermal hydrogen evolution.

INTRODUCTION

Electron transfer between multiple molecules and materials induces the formation or cleavage of chemical bonds via redox reactions. Therefore, it is vital to understand the microscopic-level behavior of electrons to ensure effective electron utilization and facilitate efficient redox reactions. Among various environmental and energy-related chemical technologies, redox reactions involved with non-thermally generated electrons at ambient temperatures, such as photocatalysis and electrocatalysis,[1-6] are more sustainable than energy-intensive thermocatalysis.

In the case of photocatalysis, photogenerated electrons reduce protons (H^+) derived from H-containing molecules, such as methane (CH_4) and water (H_2O), to produce hydrogen (H_2). Thus, photogenerated electrons are critical active species in the sustainable evolution of H_2 as an environmentally friendly energy source.[7, 8] To prolong the lifetimes of photogenerated electrons, metal cocatalysts have been generally loaded on semiconductor photocatalysts.[9] Several studies have confirmed that the loading of metal cocatalysts significantly improves the performance of semiconductor photocatalysts.[10, 11] Thus, it has been traditionally believed that metal cocatalysts sink electrons, suppress charge recombination, and function as proton reduction sites.[12, 13] However, the impact of metal cocatalyst loading on the microscopic-level behavior of reactive electrons is still poorly understood owing to the inherent challenges in the experimental observation and identification of reactive photogenerated electron species and their behavior under practical reaction conditions.

In principle, infrared (IR) spectroscopy can be conducted to nondestructively probe the amount and energy levels of photogenerated electron species. Transient IR spectroscopy has been performed to investigate the ultrafast dynamics of photogenerated electron species.[14-20] Despite intensive research,[9-20] the reactive electron species in photocatalysis remain unidentified to date. This is primarily because most transient IR studies reported to date have used excitation laser pulses with femtosecond to nanosecond duration, which do not match the timescale of reduction reactions ranging from microseconds to milliseconds.[20, 21] Furthermore, intense pulse-laser-based excitation light causes complicated carrier dynamics[22] and does not accurately represent practical reaction conditions upon the irradiation of continuous light.[8] In addition, the temperature increment for catalysts upon continuous light irradiation[23-25] impedes the identification of reactive species. Due to this temperature increment, a strong signal

corresponding to thermally excited nonreactive electron species is generated[26] and overwhelms the weak signal ascribed to the photogenerated reactive species. The substantial discrepancies in reaction conditions and intense background signals owing to sample heating make it challenging to correlate spectroscopic information with the photocatalytic performance of the system, thereby preventing the identification of reactive species.

Based on *operando* Fourier transform–infrared (FT–IR) spectroscopy, this study reports a new challenge in sensitively detecting the weak signals derived from reactive photogenerated electron species. This study is novel in that we succeeded in suppressing thermally induced nonreactive electrons while maintaining the actual photocatalytic reaction conditions, thereby providing a new direction for identifying active species in photocatalysis. Of particular importance is the adoption of the periodic photoexcitation of a sample on a reaction timescale of the order of milliseconds,[20, 21] synchronized with the period of the moving mirror of the Michelson interferometer. This technique was applied to the photocatalytic steam methane reforming on Pt- or Pd-loaded gallium oxide (Ga_2O_3) particles as model systems for photocatalytic hydrogen evolution.[27-30] By the considerable suppression of temperature variations between light-irradiated and non-irradiated conditions, we significantly reduced the intensity of the background signal originating from the thermally induced carriers not directly related to the photocatalytic reaction. Consequently, we successfully extracted and identified the signal originating from the reactive photogenerated electron species directly contributing to the hydrogen evolution reaction by correlation analyses between the IR absorption band intensity and hydrogen evolution rate (R_{H_2}). Our new microscopic insights shift a paradigm in the traditional and widespread belief on the role of metal cocatalysts in photocatalytic reduction.

RESULTS AND DISCUSSION

A well-known d^{10} photocatalyst,[2] β-Ga_2O_3, with stable activity and high robustness, was used as the model catalyst.[27, 28] For our first demonstration of *operando* observation of photogenerated electron species involved in hydrogen evolution, we focused on the photocatalytic steam methane reforming because this reaction is known to show higher H_2 formation rate than pure water splitting.[28-30] In our recent paper[29], we reported that the H_2 formation rate in pure photocatalytic water splitting under 2 kPa of water vapor with no methane gas (P_{CH_4} = 0 Pa) is approximately an order of magnitude lower than that observed in photocatalytic steam methane reforming (P_{CH_4} > 0 Pa) under 2 kPa of water vapor for the Ga_2O_3 photocatalyst, and similar features were observed also for the representative d^0 photocatalysts, such as TiO_2 and $NaTaO_3$; the Ga_2O_3 photocatalyst exhibited the highest H_2 formation rate among the three oxide species (Ga_2O_3, TiO_2 and $NaTaO_3$).[29] In the present study, Pt- and Pd-loaded particulate β-Ga_2O_3 (Pt/Ga_2O_3, Pd/Ga_2O_3) samples[29-31] were synthesized for the experiments (see Supplementary Material S1 for details). As shown in our previous study,[30] these loaded Pt and Pd cocatalysts were confirmed to be metallic through X-ray diffraction and FT–IR spectroscopy. For evaluating the photocatalytic activity, β-Ga_2O_3 with a band-gap of ~4.8 eV (~260 nm) was irradiated with a deep ultraviolet (UV) lamp (~90 mW cm^{-2} at 260± 15 nm) for excitation. The photocatalytic activities and *operando* IR spectra were measured at several P_{CH_4} under wet conditions, where the pressure of water vapor (P_{H_2O}) was fixed at 2 kPa.

Figure 1a shows the time profiles of the net temperature of Pt/Ga_2O_3 samples that were subjected to continuous UV irradiation at P_{CH_4} = 30 kPa and P_{H_2O} = 2 kPa. The continuous UV irradiation increases the temperature of metal-loaded photocatalysts by ~15 K (from ~295 K to ~310 K),[27, 32] and generates numerous thermally excited electrons.[26] As show in Figures S2-1b and S3, the absorbance signals derived from the thermally excited electron species in response to 15 K temperature rise are the order of 10^{-2}–10^{-1} and are dominantly detected on the IR spectra, obscuring the weak signals of the reactive photogenerated species (typically less than 10^{-3}). To suppress the temperature difference between illuminated and non-illuminated conditions and reduce the contribution of thermally excited electrons, we irradiated the samples with periodically chopped UV light with a period of ~200 ms (~5 Hz). This modulation period (~100 ms of irradiation and ~100 ms of non-irradiation) is sufficiently shorter than the timescale of sample heating in the order of 4 s, as indicated by the heating time profiles shown in Figures 1a and S2-1c. Then, we found that repetitive sample heating and cooling owing to the periodic excitation light modulation suppressed the average temperature rise of the sample by ~7 K (from ~295 K to ~302 K) as shown in Figure 1a. The reduction of the temperature rise approximately by half (~15 K → ~7 K) would be attributed to the decrease of the substantial UV irradiation time by half due to the chopped illumination. More importantly, we also confirmed that the instantaneous temperature difference between the illuminated and non-illuminated conditions was less than 1 K (see Supplementary Material S2 for details). In this case, we can expect that the absorbance change spectra of thermally excited electron species taken between the illuminated and non-illuminated conditions are suppressed to the order of 10^{-3}, and the signals corresponding to the reactive photogenerated species become observable as will be demonstrated in Figure 2.

Under periodically modulated excitation light, photocatalytic reactions occurred in the presence of methane gas and water vapor. At the typical reaction temperature of 302 K (Figure 1a), the P_{H_2O} value of 2 kPa corresponds to a relative humidity of ~50%, wherein the photocatalyst surfaces are covered with approximately two monolayers (MLs) of adsorbed water molecules.[29, 31] Note that the amount of produced H_2 increased almost linearly with the reaction time (Figure 1b), indicating that the photocatalytic H_2 evolution reaction proceeded under steady-state conditions within the timescale of the irradiation interval (~100 ms). Furthermore, R_{H_2} was almost independent of the excitation light modulation frequency in the range of 5–100 Hz (Figure 1b), indicating that H_2 evolution

reaction reached a steady state within 5 ms. CO_2 formation was also observed in these experiments (Figure 1b). The fourfold H_2 evolution rate relative to the CO_2 formation rate is attributed to almost stoichiometric CO_2 formation in the steam methane reforming reaction ($CH_4 + 2H_2O \rightarrow 4H_2 + CO_2$).[27-31] Note that the production rates at 5–100 Hz of modulated irradiation were almost half of those under continuous irradiation without periodic modulation (Figure S4); this is a reasonable result because the net UV irradiation time is reduced by half in the experiments using the optical chopper.

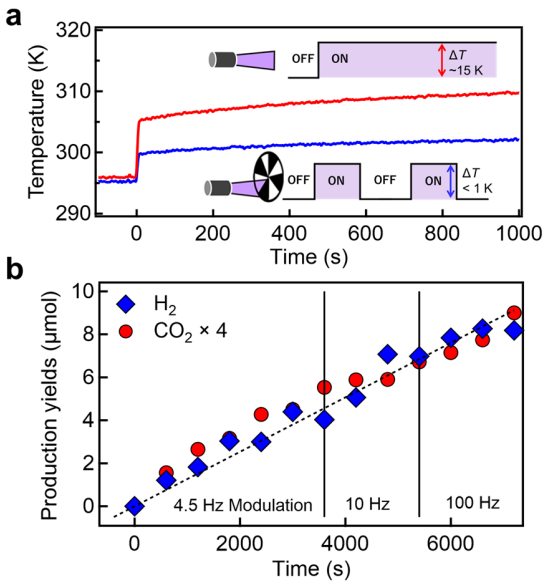

Figure 1. Effect of periodically chopped excitation light illumination on the temperature increment of the sample and the hydrogen evolution reaction. (a) Typical time profiles of the net temperature of the Pt/Ga_2O_3 photocatalyst particles subjected to (red line) continuous UV irradiation (~90 mW cm^{-2}) and (blue line) periodic UV irradiation with ~5 Hz modulation at a partial pressure of methane gas (P_{CH_4}) of 30 kPa and a partial pressure of water vapor (P_{H_2O}) of 2 kPa. Inset: Schematic of the continuous and periodic UV irradiation. During periodic UV irradiation, excitation light irradiation (ON) and non-irradiation (OFF) are periodically repeated by an optical chopper; this significantly suppresses the increase in the instantaneous temperature of the sample. (b) Time profile of the yields of H_2 and CO_2 production on the Pt/Ga_2O_3 photocatalyst at P_{CH_4} = 30 kPa and P_{H_2O} = 2 kPa. The excitation light is modulated at 5, 10, and 100 Hz at 0–3600 s, 3600–5400 s, and 5400–7200 s, respectively.

To extract the weak signals originating from the reactive photoinduced electron species while suppressing the signals derived from nonreactive thermally induced electron species under steady-state reaction conditions, we performed *operando* IR spectroscopy by synchronizing the Michelson interferometer of our FT–IR system with excitation light modulation at ~5 Hz. Figure 2a shows the absorbance-change spectra (–log (I_{on}/I_{off})) of the Pt/Ga_2O_3 samples, where I_{on} and I_{off} spectra were measured under ~100 ms illuminated and non-illuminated conditions, respectively. These spectra correspond to the changes in the *operando* IR absorbance under the reaction conditions and dark conditions. In our measurement scheme, the absorption band assigned to the thermally excited electrons in the order of 10^{-2}–10^{-1} (Figures S2-1b and S3) was significantly suppressed, and almost pure photoinduced spectral changes on the order of 10^{-3} were successfully detected (Figure 2a).

Additionally, several vibrational peaks were observed. The negative bands observed at 1630 and 2700–3700 cm^{-1} correspond to the vibrational absorption of water, specifically assigned to the H–O–H bending mode and O–H stretching mode, respectively.[17, 19] These absorption bands were attributed to bleaching due to the thermal desorption of adsorbed water caused by the temperature difference (less than 1 K) between the illuminated and non-illuminated conditions. The instantaneous temperature difference only causes a change in the amount of adsorbed water molecules of at most ~0.1 ML (see Supplementary Material S2 for details), indicating that the instantaneous thermal desorption negligibly changes the total amount of adsorbed water (~2 MLs). A positive peak observed at 1970 cm^{-1} and a side negative peak at 2040 cm^{-1} correspond to the vibrational absorption of CO on Pt,[33-35] which are reasonably considered to be assigned to the reaction intermediate species transitioning from CH_4 to CO_2.[30, 36] The bipolar spectrum shape indicates that the CO peak was red-shifted under illuminated conditions owing to the transfer of photogenerated electrons to the Pt cocatalyst[37] (see Supplementary Material S5 for details).

In addition to these sharp vibrational peaks, a broad absorbance band is detected (dotted black line in Figure 2a). The observed broad absorption band was well fitted with a linear combination of three components: a power-law curve ($\propto \tilde{\nu}^{-1.5}$) and two peaks at ~2100 and ~4200 cm^{-1} (see the bottom panel of Figure 2a and Supplementary Material S6 for details of the analysis). The power-law component was attributed to the intraband transition of free electrons[20, 38-41] possibly in the conduction band of the oxide semiconductor or in the d-band of the metallic Pt cocatalyst. Since electrons generated in the conduction band are immediately trapped at various in-gap electronic states[42] on a timescale of < 1 ps,[14-16] most of the free electron species observed on a timescale of 100 ms were reasonably assumed to be derived from the electrons in the metallic cocatalysts. Indeed, the power-law component was negligibly small under the ~100-ms periodic photoexcitation for the bare β-Ga_2O_3 samples without metal cocatalyst loading (Figure S7b).

The two peak components (~2100 and ~4200 cm^{-1}) were assigned to the IR excitation of photogenerated electrons from the discrete level of the in-gap trap states to the continuous level of the conduction band.[20, 38-41] These characteristic peak structures were also observed for the bare samples (Figure S7b); therefore, they were attributed to the photogenerated electrons trapped in the Ga_2O_3 semiconductor rather than those trapped in the Pt cocatalyst. The IR photon energy absorbed by the trapped electrons reflects the depth of the energy level of the trap states.[20, 38-41] Therefore, the two peaks at ~2100 and ~4200 cm^{-1} were

attributed to the photogenerated electrons trapped at the in-gap states that were ~0.26 and ~0.52 eV below the conduction band minimum of Ga_2O_3, respectively (see the energy diagram in Figure S6). Although the existence of the ~0.52-eV trapped state has been previously reported for the single crystals of β-Ga_2O_3,[43] shallow trap states with energies below 0.3 eV have not been confirmed experimentally[43, 44] or theoretically[45] in such single-crystal systems. However, the existence of such shallowly trapped electron species has been experimentally reported only for particulate β-Ga_2O_3,[20] indicating that the observed shallowly trapped electron species (~0.26 eV) were characteristic of the particulate β-Ga_2O_3 samples. Note that we observed these electron species in the timescale of 100 ms under chopped irradiation of UV light and confirmed that the photocatalytic reaction proceeds in this time scale (Figure 1b). In the observation time scale (100 ms), relaxation of electron species and recombination with hole species have already been achieved.[14-16] Therefore, we detected a relatively small amount of long-lived (relaxed) electron species under steady-state reaction conditions in the time scale of 100 ms. In this case, the existence of survived shallow trapped electron species indicates that the sites of shallowly and deeply trapped electrons are spatially separated.

The population of the reactive electron species contributing to photocatalytic reduction is expected to vary with the enhancement of the photocatalytic performance. Therefore, we conducted the correlation analysis between the photocatalytic performance and spectral components observed in the *operando* IR spectra. In particular, we focused on the P_{CH_4} dependence of photocatalytic performance and *operando* IR spectra to evaluate the correlation (Figure 2). As reported in literature,[29, 30] R_{H_2} for the photocatalytic steam methane reforming depends significantly on P_{CH_4} and is represented by a Langmuir-adsorption-isotherm-like curve (Figure 2b) (see also Supplementary Material S8 for details). Therefore, P_{CH_4} is a critical experimental parameter that controls the photocatalytic performance;[29, 30] thus, the absorbance-change spectra were recorded at different P_{CH_4} values. In response to the increase in R_{H_2}, the intensity of the absorption band centered at ~2100 cm^{-1} (~0.26 eV) gradually decreased, whereas the intensity of the power-law component and the peak at ~4200 cm^{-1} (~0.52 eV) remained almost unchanged with P_{CH_4} (Figures 2a and 2b). Remarkably, the free electron component in the Pt cocatalyst and the deeply trapped electron component in Ga_2O_3 were not correlated with R_{H_2}, and only the shallowly trapped electrons (e_{ST}^-) in the in-gap states of Ga_2O_3 were effectively consumed in the hydrogen evolution reaction (Figure 2c). These results indicate that the shallowly trapped electrons are reactive species that directly contribute to photocatalytic hydrogen evolution.

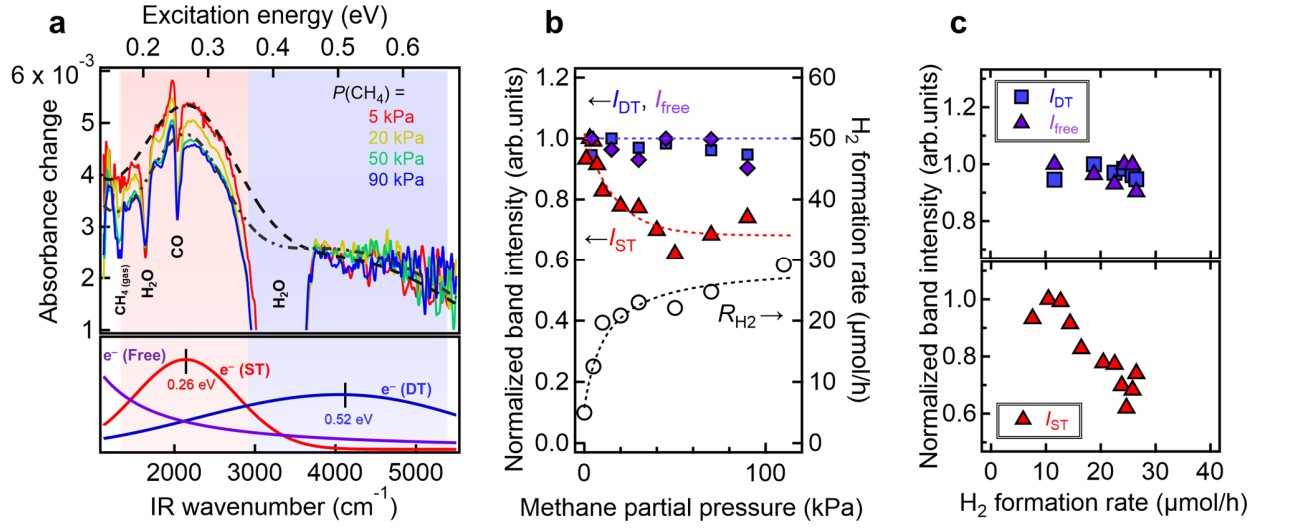

Figure 2. *Operando* IR spectra of electron species and correlations between the band intensity and hydrogen formation rates. (a) *Operando* IR absorbance-change spectra of the Pt/Ga_2O_3 samples measured under P_{H_2O} = 2 kPa and different P_{CH_4} values. Typical IR spectra of free electrons (purple), electrons in shallowly-trapped (ST) states (red), and electrons in deeply-trapped (DT) states (blue) are shown in the bottom panel. To eliminate the effect of thermal heating owing to the initial excitation light irradiation, these measurements are conducted > 30 min after the initial irradiation. (b) Intensities of absorption bands corresponding to free electrons (I_{free}), ST electrons (I_{ST}), and DT electrons (I_{DT}) as a function of P_{CH_4}. P_{CH_4} dependence of the H_2 formation rate is shown on the right axis. The dashed black line indicates the fitting analysis results based on the Langmuir-adsorption-isotherm-like curve derived from the kinetic analysis of the photocatalytic reaction (see Supplementary Material S8 and literature[29, 30] for details). (c) Correlation plots between H_2 formation rates and I_{free}, I_{ST}, and I_{DT}.

Since the early stage of the discovery of photocatalysis, it has long been believed that noble-metal cocatalysts sink reactive electrons into them.[12, 13] In contrast to the traditional belief, our results show that the free electrons in the metal cocatalysts do not directly contribute to the hydrogen evolution (Figures 2b and 2c), as few previous studies phenomenologically suggested on another metal/semiconductor photocatalytic system, Au on TiO_2.[46] This is probably because the free electrons in the metal cocatalysts are energetically relaxed[47, 48] immediately after the transfer to the metal cocatalysts and lose the ability to reduce protons. Moreover, it is conventionally expected that the metal cocatalysts assist electron–hole charge separation.[12, 13] However, as shown in Figure S7b, the intensity of the IR absorption bands corresponding to the trapped electrons was remarkably higher for the bare Ga_2O_3 samples than for the Pt/Ga_2O_3 samples. This result indicates that, even without metal cocatalysts, sufficient charge separation is achieved on the Ga_2O_3 photocatalyst in a reaction timescale of milliseconds. Although the metal cocatalyst loading does not apparently accomplish the traditionally believed abovementioned roles, we confirmed that the loading of metallic Pt does indeed promote photocatalytic reduction; R_{H_2} of Pt/Ga_2O_3 (~20 μmol h^{-1}) was more than 50 times higher than that of bare Ga_2O_3 (~0.3 μmol h^{-1}) (Figure S7a).

Then, our experimental results pose an essential question: what is the actual role of metal cocatalysts in increasing photocatalytic activity? To investigate the true mechanism underlying the improvement in the photocatalytic performance upon the loading of metal cocatalysts, we conducted activity evaluation and *operando* FT–IR spectroscopy for the Pd/Ga_2O_3 samples (Figure 3). Although Pd and Pt have been reported to be equally active electrodes for the electrochemical hydrogen evolution reaction,[49] the R_{H_2} of Pd/Ga_2O_3 (~1 μmol h^{-1}) was significantly lower than that of Pt/Ga_2O_3 (~20 μmol h^{-1}) (Figure 3a). While the intensities of the IR bands corresponding to the deeply trapped and free electrons were almost similar for these samples (Figure 3c), the intensity of the IR band attributed to the shallowly trapped electrons (~0.25 eV) for the Pd/Ga_2O_3 sample was lower than that for the Pt/Ga_2O_3 sample (Figure 3b). This clear difference suggests that Pt/Ga_2O_3 photocatalysts, which exhibit high H_2 evolution efficiency, can store more reactive electrons than the less efficient Pd/Ga_2O_3 photocatalysts. In other words, the free electrons in metal cocatalysts and deeply trapped are not involved in the hydrogen evolution reaction, and the shallowly-trapped electrons directly contribute to the photocatalytic reduction reaction. Furthermore, the P_{CH_4} dependences on the intensity of the IR band attributed to the shallowly trapped electrons for Pt/Ga_2O_3 (Figure 2a) and Pd/Ga_2O_3 (Figure S9) also vary by orders of magnitude. The observed cocatalyst-dependent differences in the storage capacity of reactive electrons generated from Ga_2O_3 states also strongly indicate that these reactive electrons were present in the vicinity of the metal cocatalyst.

Previous theoretical studies on the metal/oxide interface indicate that local band bending on the interface is distributed vertically (beneath the metal/semiconductor interface) and laterally (along the semiconductor surface).[50, 51] Lateral band bending modulates the electronic states of oxide surface sites at the periphery of loaded metal cocatalysts and influences the carrier dynamics,[52, 53] molecular adsorption,[54, 55] and catalytic reactions around the metal particles.[55-57] In our experimental results, the energy of the shallowly trapped level on the Pt/Ga_2O_3 and Pd/Ga_2O_3 samples (0.26 ± 0.05 and 0.25 ± 0.05 eV, respectively, Figure 3) was slightly shifted in relation to that on bare Ga_2O_3 samples (0.21 ± 0.10 eV, Figure S7b). This result suggests that these semiconductor surface states for the Pt/Ga_2O_3 and Pd/Ga_2O_3 samples are induced by the interaction between loaded metals and Ga_2O_3 and are present at the periphery of the metal cocatalysts. Due to the difference in the work function of the metal species, the lateral distribution range of the metal-induced semiconductor surface state derived from the lateral band bending would substantially differ between the Pt- and Pd-loaded Ga_2O_3 photocatalysts,[50] resulting in the difference in the storage capacity of reactive electrons (Figures 3b and 3c). Thus, on the basis of the discussion in this paragraph and the immediately preceding paragraph, we can reasonably conclude that the actual role of metal cocatalysts is not to store reactive free electrons in them but to provide the reactive semiconductor surface states in their surroundings.

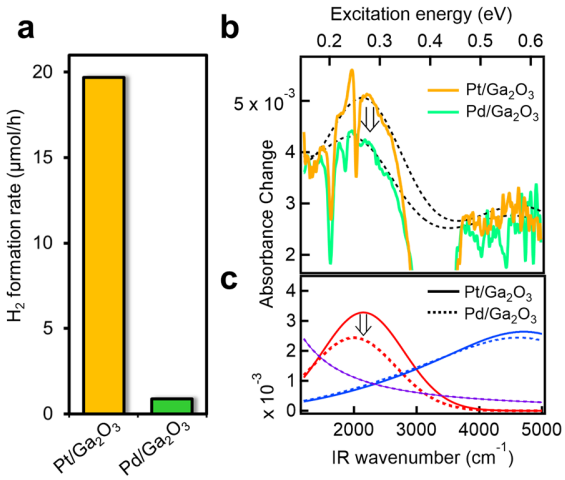

Figure 3. Hydrogen formation efficiency and *operando* IR spectra of the photogenerated electrons for Pt/Ga_2O_3 and Pd/Ga_2O_3 photocatalysts. (a) Hydrogen formation rates at P_{CH_4} = 10 kPa and P_{H_2O} = 2 kPa. (b) *Operando* IR absorbance-change spectra measured at P_{CH_4} = 10 kPa and P_{H_2O} = 2 kPa. The dashed lines indicate the results of fitting analyses with the sum of three components derived from electron species: free electrons and ST/DT electrons. (c) Decomposition of the *operando* IR absorbance-change spectra into the three components for the Pt/Ga_2O_3 (solid line) and Pd/Ga_2O_3 (dotted line) photocatalysts: absorption spectra of free electrons (purple), electrons in ST states (red), and electrons in DT states (blue).

Consequently, the photocatalytic hydrogen evolution reaction on metal-loaded Ga_2O_3 photocatalysts is reasonably assumed to proceed by the mechanism shown in Figure 4a. In the first step of this mechanism (step i), electrons and holes are generated in Ga_2O_3 by photoexcitation. Some of these electrons are trapped in the metal-induced shallow trap states of the Ga_2O_3 surface (e_{ST}^-) localized at the periphery of the metal cocatalyst at a rate constant of k_1. In the second step, these shallowly trapped electrons reduce protons derived from the oxidation of methane and water[29] and generate H atoms with rate constant k_2 (step ii: $e_{ST}^- + H^+ \rightarrow H$). Subsequently, the H atoms diffuse on the metal cocatalyst and associate to evolve H_2 in the third step (step iii: $2H \rightarrow H_2$). Simultaneously, some electrons undergo recombination at a rate constant of k_{-1} ($e_{ST}^- + h^+ \rightarrow$ *recombination*).

A kinetic analysis based on the proposed reaction model (Figure 4a) significantly rationalizes the negative correlation between R_{H_2} and the intensity of the bands attributed to the shallowly trapped electrons in the metal-induced semiconductor surface states (Figures 2b and 2c). Under steady-state reaction conditions, the increase in the number of shallowly trapped electrons by photoexcitation (step i) and the decrease due to the reduction reaction (step ii) and charge recombination were balanced as $k_1 = k_{-1}[e_{ST}^-][h^+] + k_2[e_{ST}^-][H^+]$. Moreover, the increase in the number of hydrogen atoms owing to the reduction reaction (step ii) and decrease due to the hydrogen evolution reaction (step iii) were balanced as $k_2[e_{ST}^-][H^+] = 2R_{H_2}$; factor 2 indicates that two H atoms are required for the evolution of one H_2 molecule. From these balanced equations, the following relation can be approximately derived between $[e_{ST}^-]$ and R_{H_2} (see Supplementary Material S10-1 for details):

$$[e_{ST}^-] \propto (k_1 - 2R_{H_2}). \quad (1)$$

As shown in Figure 4b, the intensity of the band attributed to the shallowly trapped electrons ($I_{ST} \propto [e_{ST}^-]$) fitted well with Equation (1), validating our experimental results and reaction model triggered by the shallowly trapped electrons (Figure 4a). Although the above reaction model (Figure 4a) assumed that the hydrogen evolution reaction proceeds through the Tafel mechanism[58] in the third reaction step ($2H \rightarrow H_2$), almost the same negative correlation (Figure 4b) is also derived for the Heyrovsky's hydrogen evolution mechanism ($H + H^+ + e_{ST}^- \rightarrow H_2$),[58] as discussed in Supplementary Material S10-2. Therefore, whether H_2 is generated from the Tafel or Heyrovsky models does not affect our primary conclusion regarding the identification of the reactive electron species.

Finally, it is worth noting that although the photocatalysts exhibited the maximal and saturated photocatalytic performance at $P_{CH_4} > 40$ kPa, the IR absorption band of the shallowly trapped electrons still remained, and the reactive electron species were not fully consumed (Figures 2 and 4b). An extension of the fitting line in Figure 4b indicates that the photocatalytic performance should be more than double (an increase from ~30 to ~65 μmol h^{-1}) if all the shallowly trapped electrons are completely consumed (Figure S10). Thus, the reaction activity has been saturated though excess reactive electrons are still present in the photocatalytic systems. Although most studies on photocatalysis have considered the promotion of charge separation to be the key to high photocatalytic performance,[3, 59] our results clearly show that sufficient charge separation is already achieved on the Ga_2O_3 photocatalysts, and surplus reactive electrons remain at the metal/oxide interface. Therefore, further promotion of charge separation would have a negligible impact on the improvement of photocatalytic performance. To efficiently utilize the surplus electrons and further enhance the photocatalytic performance, sufficient protons would have to be supplied to the reactive sites by accelerating the oxidation processes ($CH_4 + h^+ \rightarrow H^+ + {}^{\bullet}CH_3$; $H_2O + h^+ \rightarrow H^+ + {}^{\bullet}OH$).[29]

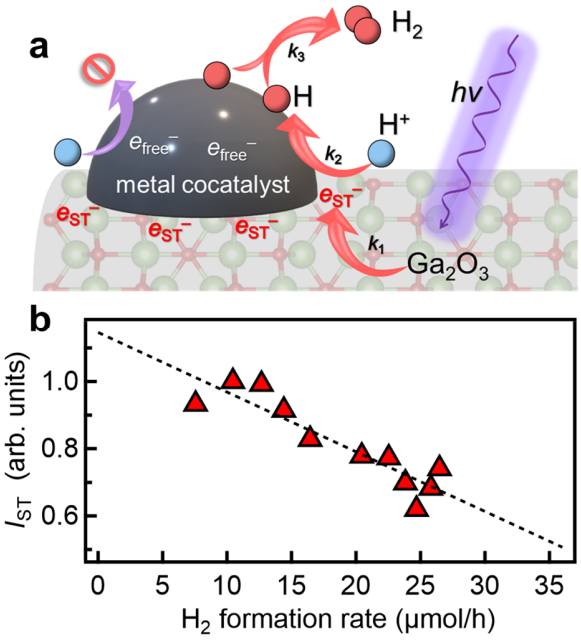

Figure 4. (a) Schematic illustration of how the ST electrons contribute to photocatalytic H_2 evolution reaction. This reaction is initiated by the reduction of protons by the ST electrons on the metal-induced semiconductor surface states at the periphery of the metal cocatalysts. The H atoms produced in the reduction reaction diffuse on the metal cocatalyst and associate to evolve H_2 molecules. (b) Correlation between I_{ST} and H_2 formation rate on the Pt/Ga_2O_3 photocatalyst. The dashed line shows the curve-fitting results using Equation (1).

CONCLUSIONS

It is critical to explore the factors degrading the performance of the currently employed photocatalytic systems and those inhibiting further improvement of the reaction activity. Without such microscopic knowledge, it is difficult to design effective strategies for the development of more sophisticated catalysts and suitable surface reaction sites. This study reported a promising *operando* spectroscopy technique for extracting weak signals assigned to reactive photogenerated species under realistic working conditions. This innovation was achieved by synchronizing

the millisecond periodic excitation of the photocatalyst with the scanning rate of the Michelson interferometer used for FT–IR spectroscopy. The periodic light irradiation successfully suppressed intense background signals originating from thermally excited electrons, and the weak signals corresponding to photogenerated species were detected with high sensitivity. On adopting the proposed technique to the photocatalytic hydrogen evolution reaction on metal-loaded Ga_2O_3 samples, we found that the signal assigned to the free electrons trapped in the metal cocatalysts did not correlate with the hydrogen evolution efficiency, despite a significant increase in R_{H_2} owing to metal cocatalyst loading. This indicates that the free electrons in the metal cocatalysts did not contribute to the hydrogen evolution reaction, contrary to the traditional belief that metal cocatalysts themselves function as sinks for reactive electrons. Instead, our experimental results strongly suggested that the shallowly trapped electron species[46] at the metal-induced Ga_2O_3 surface states formed in the periphery of the loaded metal cocatalysts functioned as reactive electrons, directly contributing to the reduction of protons to hydrogen atoms ($e_{ST}^- + H^+ \rightarrow H$); the lateral boundaries between loaded metals and oxide substrate are promising platforms for driving non-thermal reduction reactions. Intriguingly, even when the reaction activity was maximized and saturated approximately at ambient methane pressure (P_{CH_4} > 40 kPa), the excess reactive electrons remained at the metal/oxide interface. This observation indicates that the supply of sufficient protons is vital for further improving the photocatalytic performance of the metal-loaded Ga_2O_3 samples. Our concept of *operando* spectroscopy combined with millisecond-scale excitation can be applicable not only to other photocatalytic systems, such as pure water splitting, but also to other various nonthermal redox reaction systems, including electrocatalysis[5] and electric-field-assisted catalysis[6] for microscopically elucidating key factors for achieving high catalytic performance.

ASSOCIATED CONTENT

Supporting Information. Experimental; Evaluation of sample heating due to UV light irradiation; Temperature dependence of IR signals derived from thermally excited electrons; Effect of periodic UV irradiation on photocatalytic performance; IR spectra for gaseous and adsorbed molecules; Fitting analysis of IR spectra for electron species; Comparison of R_{H_2} and *operando* IR spectra for bare and Pt-loaded Ga_2O_3 samples; Derivation of relationship between R_{H_2} and P_{CH_4} based on kinetic analysis; IR spectra of Pd/Ga_2O_3 samples under periodic UV irradiation; Derivation of relationship between I_{ST} and R_{H_2} based on kinetic analysis; IR spectra of Pt/Ga_2O_3 samples under inert Ne gas. These materials are available free of charge at http://pubs.acs.org.

AUTHOR INFORMATION

Corresponding Author

Toshiki Sugimoto – Department of Materials Molecular Science, Institute for Molecular Science, Okazaki, Aichi 444-8585, Japan; Graduate Institute for Advanced Studies, SOKENDAI, Okazaki, Aichi 444-8585, Japan; ORCID: http://orcid.org/0000-0003-3453-6009; E-mail: toshiki-sugimoto@ims.ac.jp

Notes

The authors declare no competing financial interest.

ACKNOWLEDGMENT

This work was supported by JST-PRESTO [No. JPMJPR16S7], JSPS KAKENHI Grant-in-Aid for Scientific Research (A) [No. JP22H00296], Grant-in-Aid for JSPS Fellows [No. JP22KJ1427], and Joint Research by the National Institutes of Natural Sciences (NINS) [No. 01112104]. This work was also partially supported by JST-CREST [No. JPMJCR22L2] and Demonstration Project of Innovative Catalyst Technology for Decarbonization through Regional Resource Recycling, the Ministry of the Environment, Government of Japan. A part of this work was performed with the aid of Equipment Development Center and Instrument Center, Institute for Molecular Science. The authors acknowledge Mr. Taisuke Higashi, Dr. Hikaru Saito, Kotaro Takeyasu, Akira Yamamoto, Hisao Yoshida, Fumiaki Kato, Norihiro Aiga, Susumu Saito, Kazuya Watanabe, Yoshiyasu Matsumoto, and Atsunori Sakurai for fruitful discussion and/or contribution in the early stage of this research.

REFERENCES

(1) Fujishima, A.; Honda, K. Electrochemical Photolysis of Water at a Semiconductor Electrode. *Nature* **1972**, *238* (5358), 37–38. DOI: 10.1038/238037a0.

(2) Kudo, A.; Miseki, Y. Heterogeneous Photocatalyst Materials for Water Splitting. *Chem. Soc. Rev.* **2009**, *38* (1), 253–278. DOI: 10.1039/b800489g.

(3) Wang, Q.; Domen, K. Particulate Photocatalysts for Light-Driven Water Splitting: Mechanisms, Challenges, and Design Strategies. *Chem. Rev.* **2020**, *120* (2), 919–985. DOI: 10.1021/acs.chemrev.9b00201.

(4) Yamauchi, M.; Saito, H.; Sugimoto, T.; Mori, S.; Saito, S. Sustainable Organic Synthesis Promoted on Titanium Dioxide Using Coordinated Water and Renewable Energies/resources. *Coord. Chem. Rev.* **2022**, *472*, 214773. DOI: 10.1016/j.ccr.2022.214773.

(5) Seh, Z. W.; Kibsgaard, J.; Dickens, C. F.; Chorkendorff, I.; Nørskov, J. K.; Jaramillo, T. F. Combining Theory and Experiment in Electrocatalysis: Insights into Materials Design. *Science* **2017**, *355* (6321), eaad4998. DOI: 10.1126/science.aad4998.

(6) Hisai, Y.; Ma, Q.; Qureishy, T.; Watanabe, T.; Higo, T.; Norby, T.; Sekine, Y. Enhanced Activity of Catalysts on Substrates with Surface Protonic Current in an Electrical Field – A Review. *Chem. Commun.* **2021**, *57* (47), 5737–5749. DOI: 10.1039/d1cc01551f.

(7) Zhu, J.; Hu, L.; Zhao, P.; Lee, L. Y. S.; Wong, K.-Y. Recent Advances in Electrocatalytic Hydrogen Evolution Using Nanoparticles. *Chem. Rev.* **2020**, *120* (2), 851–918. DOI: 10.1021/acs.chemrev.9b00248.

(8) Nishiyama, H.; Yamada, T.; Nakabayashi, M.; Maehara, Y.; Yamaguchi, M.; Kuromiya, Y.; Nagatsuma, Y.; Tokudome, H.; Akiyama, S.; Watanabe, T.; et al. Photocatalytic Solar Hydrogen Production from Water on a 100-m² Scale. *Nature* **2021**, *598* (7880), 304–307. DOI: 10.1038/s41586-021-03907-3.

(9) Zhu, J.; Pang, S.; Dittrich, T.; Gao, Y.; Nie, W.; Cui, J.; Chen, R.; An, H.; Fan, F.; Li, C. Visualizing the Nano Cocatalyst Aligned Electric Fields on Single Photocatalyst Particles. *Nano Lett.* **2017**, *17* (11), 6735–6741. DOI: 10.1021/acs.nanolett.7b02799.

(10) Maeda, K.; Teramura, K.; Lu, D.; Saito, N.; Inoue, Y.; Domen, K. Noble-Metal/Cr_2O_3 Core/Shell Nanoparticles as a Cocatalyst

for Photocatalytic Overall Water Splitting. *Angew. Chem. Int. Ed.* **2006**, *45* (46), 7806–7809. DOI: 10.1002/anie.200602473.

(11) Leung, D. Y. C.; Fu, X.; Wang, C.; Ni, M.; Leung, M. K. H.; Wang, X.; Fu, X. Hydrogen Production over Titania-Based Photocatalysts. *ChemSusChem* **2010**, *3* (6), 681–694. DOI: 10.1002/cssc.201000014.

(12) Yang, J.; Wang, D.; Han, H.; Li, C. Roles of Cocatalysts in Photocatalysis and Photoelectrocatalysis. *Acc. Chem. Res.* **2013**, *46* (8), 1900–1909. DOI: 10.1021/ar300227e.

(13) Meng, A.; Zhang, L.; Cheng, B.; Yu, J. Dual Cocatalysts in TiO_2 Photocatalysis. *Adv. Mater.* **2019**, 1807660. DOI: 10.1002/adma.201807660.

(14) Skinner, D. E.; Colombo, D. P.; Cavaleri, J. J.; Bowman, R. M. Femtosecond Investigation of Electron Trapping in Semiconductor Nanoclusters. *J. Phys. Chem.* **1995**, *99* (20), 7853–7856. DOI: 10.1021/j100020a003.

(15) Iwata, K.; Takaya, T.; Hamaguchi, H.-O.; Yamakata, A.; Ishibashi, T.-A.; Onishi, H.; Kuroda, H. Carrier Dynamics in TiO_2 and Pt/TiO_2 Powders Observed by Femtosecond Time-Resolved Near-Infrared Spectroscopy at a Spectral Region of 0.9–1.5 μm with the Direct Absorption Method. *J. Phys. Chem. B* **2004**, *108* (52), 20233–20239. DOI: 10.1021/jp047531k.

(16) Tamaki, Y.; Furube, A.; Murai, M.; Hara, K.; Katoh, R.; Tachiya, M. Dynamics of Efficient Electron–hole Separation in TiO_2 Nanoparticles Revealed by Femtosecond Transient Absorption Spectroscopy under the Weak-excitation Condition. *Phys. Chem. Chem. Phys.* **2007**, *9* (12), 1453–1460. DOI: 10.1039/B617552J.

(17) Shirai, K.; Sugimoto, T.; Watanabe, K.; Haruta, M.; Kurata, H.; Matsumoto, Y. Effect of Water Adsorption on Carrier Trapping Dynamics at the Surface of Anatase TiO_2 Nanoparticles. *Nano Lett.* **2016**, *16* (2), 1323–1327. DOI: 10.1021/acs.nanolett.5b04724.

(18) Vequizo, J. J. M.; Matsunaga, H.; Ishiku, T.; Kamimura, S.; Ohno, T.; Yamakata, A. Trapping-Induced Enhancement of Photocatalytic Activity on Brookite TiO_2 Powders: Comparison with Anatase and Rutile TiO_2 Powders. *ACS Catal.* **2017**, *7* (4), 2644–2651. DOI: 10.1021/acscatal.7b00131.

(19) Shirai, K.; Fazio, G.; Sugimoto, T.; Selli, D.; Ferraro, L.; Watanabe, K.; Haruta, M.; Ohtani, B.; Kurata, H.; Di Valentin, C.; et al. Water-Assisted Hole Trapping at the Highly Curved Surface of Nano-TiO_2 Photocatalyst. *J. Am. Chem. Soc.* **2018**, *140* (4), 1415–1422. DOI: 10.1021/jacs.7b11061.

(20) Yamakata, A.; Vequizo, J. J. M.; Ogawa, T.; Kato, K.; Tsuboi, S.; Furutani, N.; Ohtsuka, M.; Muto, S.; Kuwabara, A.; Sakata, Y. Core–Shell Double Doping of Zn and Ca on β-Ga_2O_3 Photocatalysts for Remarkable Water Splitting. *ACS Catal.* **2021**, *11* (4), 1911–1919. DOI: 10.1021/acscatal.0c05104.

(21) Takanabe, K. Addressing Fundamental Experimental Aspects of Photocatalysis Studies. *J. Catal.* **2019**, *370*, 480–484. DOI: 10.1016/j.jcat.2018.10.006.

(22) Jursenas, S.; Stepankevicius, V.; Strumskis, M.; Zukauskas, A. Carrier Recombination in CdS Nanocrystals under Single-electron and High-density Excitation. *Semicond. Sci. Technol.* **1995**, *10* (3), 302–309. DOI: 10.1088/0268-1242/10/3/011.

(23) Miao, T. J.; Wang, C.; Xiong, L.; Li, X.; Xie, J.; Tang, J. In Situ Investigation of Charge Performance in Anatase TiO_2 Powder for Methane Conversion by Vis–NIR Spectroscopy. *ACS Catal.* **2021**, *11*, 8226–8238. DOI: 10.1021/acscatal.1c01998.

(24) Fu, Z.; Hirai, T.; Onishi, H. Long-Life Electrons in Metal-Doped Alkali-Metal Tantalate Photocatalysts Excited under Water. *J. Phys. Chem. C* **2021**, *125* (48), 26398–26405. DOI: 10.1021/acs.jpcc.1c06618.

(25) Litke, A.; Su, Y.; Tranca, I.; Weber, T.; Hensen, E. J. M.; Hofmann, J. P. Role of Adsorbed Water on Charge Carrier Dynamics in Photoexcited TiO_2. *J. Phys. Chem. C* **2017**, *121* (13), 7514–7524. DOI: 10.1021/acs.jpcc.7b00472.

(26) Sato, H.; Sugimoto, T. Operando FT-IR Spectroscopy of Steam-methane-reforming Photocatalyst under Irradiation of Intensity Modulated UV Light. *Vac. Surf. Sci.* **2020**, *63* (9), 476–481. DOI: 10.1380/vss.63.476.

(27) Shimura, K.; Yoshida, T.; Yoshida, H. Photocatalytic Activation of Water and Methane over Modified Gallium Oxide for Hydrogen Production. *J. Phys. Chem. C* **2010**, *114* (26), 11466–11474. DOI: 10.1021/jp1012126.

(28) Amano, F.; Akamoto, C.; Ishimaru, M.; Inagaki, S.; Yoshida, H. Pressure-induced Dehydrogenative Coupling of Methane to Ethane by Platinum-loaded Gallium Oxide Photocatalyst. *Chem. Commun.* **2020**, *56* (47), 6348–6351. DOI: 10.1039/D0CC01730B.

(29) Sato, H.; Ishikawa, A.; Saito, H.; Higashi, T.; Takeyasu, K.; Sugimoto, T. Critical Impacts of Interfacial Water on C–H Activation in Photocatalytic Methane Conversion. *Commun. Chem.* **2023**, *6*, 8. DOI: 10.1038/s42004-022-00803-3.

(30) Saito, H.; Sato, H.; Higashi, T.; Sugimoto, T. Beyond Reduction Cocatalysts: Critical Role of Metal Cocatalysts in Photocatalytic Oxidation of Methane with Water. *Angew. Chem. Int. Ed.* **2023**, *62* (33), e202306058. DOI: 10.1002/anie.202306058.

(31) Amano, F.; Ishikawa, A.; Sato, H.; Akamoto, C.; Singh, S. P.; Yamazoe, S.; Sugimoto, T. Facilitating Methane Conversion and Hydrogen Evolution on Platinized Gallium Oxide Photocatalyst through Liquid-like Water Nanofilm Formation. *Catal. Today* **2024**, *426*, 114375. DOI: 10.1016/j.cattod.2023.114375.

(32) Szczepankiewicz, S. H.; Moss, J. A.; Hoffmann, M. R. Slow Surface Charge Trapping Kinetics on Irradiated TiO_2. *J. Phys. Chem. B* **2002**, *106* (11), 2922–2927. DOI: 10.1021/jp004244h.

(33) Aleksandrov, H. A.; Neyman, K. M.; Hadjiivanov, K. I.; Vayssilov, G. N. Can the State of Platinum Species be Unambiguously Determined by the Stretching Frequency of an Adsorbed CO Probe Molecule? *Phys. Chem. Chem. Phys.* **2016**, *18* (32), 22108–22121. DOI: 10.1039/c6cp03988j.

(34) Avanesian, T.; Dai, S.; Kale, M. J.; Graham, G. W.; Pan, X.; Christopher, P. Quantitative and Atomic-Scale View of CO-Induced Pt Nanoparticle Surface Reconstruction at Saturation Coverage via DFT Calculations Coupled with in Situ TEM and IR. *J. Am. Chem. Soc.* **2017**, *139* (12), 4551–4558. DOI: 10.1021/jacs.7b01081.

(35) Yoshinobu, J.; Kawai, M. Initial Adsorption Sites of CO on Pt(111) and Ni(100) at Low Temperature. *Surf. Sci.* **1996**, *363* (1), 105–111. DOI: 10.1016/0039-6028(96)00117-3.

(36) Psofogiannakis, G.; St-Amant, A.; Ternan, M. Methane Oxidation Mechanism on Pt(111): A Cluster Model DFT Study. *J. Phys. Chem. B* **2006**, *110* (48), 24593–24605. DOI: 10.1021/jp061559.

(37) Yoshida, M.; Yamakata, A.; Takanabe, K.; Kubota, J.; Osawa, M.; Domen, K. ATR-SEIRAS Investigation of the Fermi Level of Pt Cocatalyst on a GaN Photocatalyst for Hydrogen Evolution under Irradiation. *J. Am. Chem. Soc.* **2009**, *131* (37), 13218–13219. DOI: 10.1021/ja904991p.

(38) Pankove, J. I. *Optical Processes in Semiconductors*; Dover, 1971; pp 34–86.

(39) Yamakata, A.; Ishibashi, T. A.; Onishi, H. Time-resolved Infrared Absorption Spectroscopy of Photogenerated Electrons in Platinized TiO_2 Particles. *Chem. Phys. Lett.* **2001**, *333* (3-4), 271–277. DOI: 10.1016/S0009-2614(00)01374-9.

(40) Yamakata, A.; Kawaguchi, M.; Nishimura, N.; Minegishi, T.; Kubota, J.; Domen, K. Behavior and Energy States of Photogenerated Charge Carriers on Pt- or CoO_x-Loaded $LaTiO_2N$ Photocatalysts: Time-Resolved Visible to Mid-Infrared Absorption Study. *J. Phys. Chem. C* **2014**, *118* (41), 23897–23906. DOI: 10.1021/jp5082332.

(41) Yoshihara, T.; Katoh, R.; Furube, A.; Tamaki, Y.; Murai, M.; Hara, K.; Murata, S.; Arakawa, H.; Tachiya, M. Identification of Reactive Species in Photoexcited Nanocrystalline TiO_2 Films by Wide-Wavelength-Range (400–2500 nm) Transient Absorption

Spectroscopy. *J. Phys. Chem. B* **2004**, *108* (12), 3817–3823. DOI: 10.1021/jp031305d.

(42) Nitta, A.; Takase, M.; Takashima, M.; Murakami, N.; Ohtani, B. A Fingerprint of Metal-oxide Powders: Energy-resolved Distribution of Electron Traps. *Chem. Commun.* **2016**, *52* (81), 12096–12099. DOI: 10.1039/c6cc04999k.

(43) Irmscher, K.; Galazka, Z.; Pietsch, M.; Uecker, R.; Fornari, R. Electrical Properties of β-Ga_2O_3 Single Crystals Grown by the Czochralski Method. *J. Appl. Phys.* **2011**, *110* (6), 063720–063720. DOI: 10.1063/1.3642962.

(44) Zhang, Z.; Farzana, E.; Arehart, A. R.; Ringel, S. A. Deep Level Defects throughout the Bandgap of (010) β-Ga_2O_3 Detected by Optically and Thermally Stimulated Defect Spectroscopy. *Appl. Phys. Lett.* **2016**, *108* (5), 052105. DOI: 10.1063/1.4941429.

(45) Deák, P.; Duy Ho, Q.; Seemann, F.; Aradi, B.; Lorke, M.; Frauenheim, T. Choosing the Correct Hybrid for Defect Calculations: A Case Study on Intrinsic Carrier Trapping in β–Ga_2O_3. *Phys. Rev. B* **2017**, *95* (7), 075208–075208. DOI: 10.1103/PhysRevB.95.075208.

(46) Joo, J. B.; Dillon, R.; Lee, I.; Yin, Y.; Bardeen, C. J.; Zaera, F. Promotion of Atomic Hydrogen Recombination as an Alternative to Electron Trapping for the Role of Metals in the Photocatalytic Production of H_2. *Proc. Nat. Acad. Sci.* **2014**, *111* (22), 7942–7947. DOI: 10.1073/pnas.1405365111.

(47) Schoenlein, R. W.; Fujimoto, J. G.; Eesley, G. L.; Capehart, T. W. Femtosecond Studies of Image-Potential Dynamics in Metals. *Phys. Rev. Lett.* **1988**, *61* (22), 2596–2599. DOI: 10.1103/physrevlett.61.2596.

(48) Borgwardt, M.; Omelchenko, S. T.; Favaro, M.; Plate, P.; Höhn, C.; Abou-Ras, D.; Schwarzburg, K.; Van De Krol, R.; Atwater, H. A.; Lewis, N. S.; et al. Femtosecond Time-resolved Two-photon Photoemission Studies of Ultrafast Carrier Relaxation in Cu_2O Photoelectrodes. *Nat. Commun.* **2019**, *10*, 2106. DOI: 10.1038/s41467-019-10143-x.

(49) Nørskov, J. K.; Bligaard, T.; Logadottir, A.; Kitchin, J. R.; Chen, J. G.; Pandelov, S.; Stimming, U. Trends in the Exchange Current for Hydrogen Evolution. *J. Electrochem. Soc.* **2005**, *152* (3), J23. DOI: 10.1149/1.1856988.

(50) Ioannides, T.; Verykios, X. E. Charge Transfer in Metal Catalysts Supported on Doped TiO_2: A Theoretical Approach Based on Metal-semiconductor Contact Theory. *J. Catal.* **1996**, *161* (2), 560–569. DOI: 10.1006/jcat.1996.0218.

(51) Donolato, C. Approximate Analytical Solution to the Space Charge Problem in Nanosized Schottky Diodes. *J. Appl. Phys.* **2004**, *95* (4), 2184–2186. DOI: 10.1063/1.1641516.

(52) Zachman, M. J.; Fung, V.; Polo-Garzon, F.; Cao, S.; Moon, J.; Huang, Z.; Jiang, D.-E.; Wu, Z.; Chi, M. Measuring and Directing Charge Transfer in Heterogenous Catalysts. *Nat. Commun.* **2022**, *13*, 3253. DOI: 10.1038/s41467-022-30923-2.

(53) Muhich, C. L.; Zhou, Y.; Holder, A. M.; Weimer, A. W.; Musgrave, C. B. Effect of Surface Deposited Pt on the Photoactivity of TiO_2. *J. Phys. Chem. C* **2012**, *116* (18), 10138–10149. DOI: 10.1021/jp301862m.

(54) Iwase, A.; Kato, H.; Kudo, A. The Effect of Au Cocatalyst Loaded on La-doped $NaTaO_3$ on Photocatalytic Water Splitting and O_2 Photoreduction. *Appl. Catal., B* **2013**, *136*, 89–93. DOI: 10.1016/j.apcatb.2013.02.006.

(55) Widmann, D.; Behm, R. J. Activation of Molecular Oxygen and the Nature of the Active Oxygen Species for CO Oxidation on Oxide Supported Au Catalysts. *Acc. Chem. Res.* **2014**, *47* (3), 740–749. DOI: 10.1021/ar400203e.

(56) Zhang, Z.; Yates, J. T. Band Bending in Semiconductors: Chemical and Physical Consequences at Surfaces and Interfaces. *Chem. Rev.* **2012**, *112* (10), 5520–5551. DOI: 10.1021/cr3000626.

(57) Larmier, K.; Liao, W. C.; Tada, S.; Lam, E.; Verel, R.; Bansode, A.; Urakawa, A.; Comas - Vives, A.; Copéret, C. CO_2 - to - Methanol Hydrogenation on Zirconia - Supported Copper Nanoparticles: Reaction Intermediates and the Role of the Metal–Support Interface. *Angew. Chem. Int. Ed.* **2017**, *56* (9), 2318–2323. DOI: 10.1002/anie.201610166.

(58) Zheng, Y.; Jiao, Y.; Jaroniec, M.; Qiao, S. Z. Advancing the Electrochemistry of the Hydrogen - Evolution Reaction through Combining Experiment and Theory. *Angew. Chem. Int. Ed.* **2015**, *54* (1), 52–65. DOI: 10.1002/anie.201407031.

(59) Chen, R.; Ren, Z.; Liang, Y.; Zhang, G.; Dittrich, T.; Liu, R.; Liu, Y.; Zhao, Y.; Pang, S.; An, H.; et al. Spatiotemporal Imaging of Charge Transfer in Photocatalyst Particles. *Nature* **2022**, *610* (7931), 296–301. DOI: 10.1038/s41586-022-05183-1.